Agricultural and Forest Meteorology 150 (2010) 361–368

Contents lists available at ScienceDirect

Agricultural and Forest Meteorology

journal homepage: www.elsevier.com/locate/agrformet

Diffuse radiation and cloud fraction relationships in two contrasting Amazonian rainforest sites

Nathalie Butt [a,*], Mark New [b], Yadvinder Malhi [a], Antonio Carlos Lôla da Costa [c], Paulo Oliveira [c], Javier Eduardo Silva-Espejo [d]

[a] Environmental Change Institute, School of Geography and the Environment, University of Oxford, UK
[b] School of Geography and the Environment, University of Oxford, UK
[c] Universidade Federal do Pará, Centro de Geociencias, Belém, Pará, Brazil
[d] Universidad San Antonio Abad, Cusco, Peru

ARTICLE INFO

Article history:
Received 2 December 2008
Received in revised form 19 October 2009
Accepted 11 December 2009

Keywords:
Amazon
Solar radiation
Tropical forest
Cloud fraction
Diffuse radiation

ABSTRACT

Along with total radiation received, the proportion of diffuse to direct solar radiation can influence forest photosynthesis and carbon cycling. However, tropical diffuse radiation regimes are poorly described, and to date there are few or no site-based or regional diffuse radiation datasets. The relationship between cloud fraction and diffuse solar radiation was investigated using data from two sites in western and eastern Amazonia. Radiation regimes for diffuse and total radiation were characterised for each site, and the variation in clear sky diffuse radiation fraction between wet and dry season demonstrated and quantified, as well as the dependence of diffuse radiation on cloud amount. Using high frequency measurements of diffuse and total solar radiation data from the two sites, and estimated top of the canopy clear-sky radiation, a number of alternative models to predict diffuse radiation fraction from cloud fraction were formulated and tested. Results showed that cloud fraction can be approximated using the relationship between observed and calculated top of canopy radiation, after which diffuse radiation can then be predicted from cloud fraction. We also demonstrate that satellite cloud data (from the International Satellite Cloud Climatology Project) can be used as inputs to the diffuse radiation model to provide estimates of annual and monthly diffuse radiation proportion.

© 2009 Elsevier B.V. All rights reserved.

1. Introduction

Forest canopies receive direct and diffuse solar radiation, the latter scattered by clouds, haze or other atmospheric particles and aerosols. The differential response of vegetation – such as in terms of seedling crown orientation and light interception – to diffuse and direct radiation has been documented for many years (Ackerley and Bazzaz, 1995). It has also been shown that vegetation productivity is sensitive to fluctuations in diffuse radiation, which is used more efficiently than direct radiation (Weiss and Norman, 1985; Roderick et al., 2001). Because of its multitude of incidence angles, diffuse radiation can penetrate deeper into the light-limited lower canopy, and hence stimulate photosynthesis and productivity. In tropical forests, dry season CO_2 uptake seems to be amplified by the presence of atmospheric aerosols (Oliveira et al., 2007), which increase diffuse radiation. There are indications that forest productivity in Amazonia has increased over the last two decades (Phillips et al., 2002, 2004; Lewis et al., 2004), and one suggestion is that these trends may be partially explained by changes in light regime (e.g., Nemani et al., 2003). Elucidating more fully the role played by diffuse radiation may be a crucial part of understanding how and why this is happening.

Changes in ecosystem productivity are difficult to understand in terms of climate, as there are frequently large-scale mismatches between ecological observations (e.g., monitoring plots) and climate data. In the absence of co-located meteorological data, climate-ecological relationships are frequently inferred from coarser resolution climate datasets. For diffuse radiation, however, there are no large-scale datasets, and instrumental measurements have largely been concentrated in northern hemisphere temperate regions. Currently there are no published diffuse radiation data for tropical forest regions such as Amazonia, our area of focus.

Previous approaches to estimating diffuse radiation use the ratio of ground to top-of-the-atmosphere (TOA) direct radiation (or 'clearness index'; see Liu and Jordan, 1960; Orgill and Hollands, 1977; Collares-Pereira and Rabl, 1979; Erbs et al., 1982; Spitters et al., 1986). This relies on there being a relationship between diffuse fraction (diffuse/total radiation at the surface) and atmospheric transmission (total surface versus TOA radiation),

* Corresponding author.
E-mail address: nathalie.butt@eci.ox.ac.uk (N. Butt).

0168-1923/$ – see front matter © 2009 Elsevier B.V. All rights reserved.
doi:10.1016/j.agrformet.2009.12.004

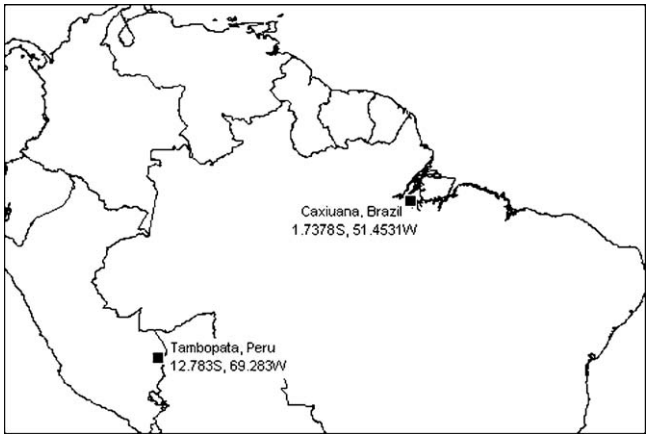

Fig. 1. Location of the study sites.

with diffuse fraction (S_d/S_t) being negatively correlated with atmospheric transmission. The advantage of this method for derivation of the clearness index is that it requires only one observed or recorded input, that of total radiation at the surface. The total TOA radiation (S_{po}) can be calculated (using, for example, the Campbell and Norman, 1998, formulation), and thence atmospheric transmission, S_t/S_{po}, or clearness index (also known as k_t, defined at), can be derived. Weiss and Norman (1985) further specifically considered the issue of leaf spectral responses to near-infrared and photosynthetically active radiation (PAR) separately for direct and diffuse radiation, which aimed to account for the variation in radiation within the canopy environment. More recently Muneer and Munawwar (2006) tested possible methods of improving this regression model calculation for diffuse radiation at northern hemisphere sites in Europe and Asia, by including various meteorological parameters, such as sunshine fraction (the daily percentage of bright sunshine time), air mass (from atmospheric thickness) and cloud fraction (the portion of the sky that is covered by clouds). Their results showed that taking account of sunshine or cloud fraction greatly improved the accuracy of prediction of diffuse radiation.

We propose that it should be possible to derive a quantitative relationship between cloud fraction and diffuse radiation measured at a few sites, which can then be applied across the Amazonian region. The relationship between diffuse radiation and total radiation at the surface is a well-defined one (cf. Spitters et al., 1986; Gopinathan and Soler, 1995; Roderick, 1999) and is central to this work. We utilise two sets of measurements of radiation data from field sites in Amazonian rainforests, recorded at a fixed weather station in Brazil and collected from a dry-season field campaign in Peru. To our knowledge, these are the only such high temporal-resolution diffuse radiation available for this region, and provide a unique opportunity to explore the diffuse radiation characteristics of contrasting sites in the Amazon. Cloud fraction is itself derived from total radiation measurements using a new technique of exploiting high time-resolution weather data.

The aims of our study are: (1) to derive a ground-based record of cloud fraction using high-frequency solar radiation data; (2) to develop a model to predict diffuse radiation from cloud fraction, and; (3) to validate satellite cloud products with ground observations of cloud fraction and test whether satellite-derived cloud fraction data can be a useful predictor of diffuse radiation.

Section 2 introduces the forest sites and data sources; Section 3 describes the radiation regimes at the two sites. In Section 4 we characterise the relationship between the cloud fraction and diffuse radiation proportion and explore the seasonal and monthly variation in the regression parameters. Section 5 describes the development and testing of the regression model and in Section 6 we go on to investigate the use of satellite cloud fraction data in the model. The final section gives an overview of the model and our conclusions.

2. Study area and radiation data

We use diffuse radiation data collected from two sites in east and west Amazonia (Fig. 1: Table 1). At Caxiuaña, Brazil, diffuse (S_d) and total (S_t) PAR radiation data were collected using a BF3 sunshine sensor (from Delta-T Devices, Cambridge, UK, as evaluated by Wood et al., 2003) located at a height of 50 m, about 20 m above a tropical rainforest. The data were recorded as μmol m^{-2} s^{-2} and converted to W m^{-2} by multiplying by 0.5.

At Tambopata, Peru, a HOBO weather station (Onset Corporation) has recorded total radiation for a number of years, but diffuse radiation has not been not routinely recorded. A BF3 sunshine sensor was installed adjacent to the existing HOBO weather station over a three-week period in the 2006 early dry season (July). The HOBO station was situated in a forest clearing and thus was affected by shading from the surrounding canopy in early morning and evening: data from these periods of the day are excluded from further analysis. The sunshine sensor was in position for the seven hours a day when the clearing was not shaded by surrounding vegetation, and the HOBO weather station recorded continuously. The sunshine sensor recorded S_d and S_t at one minute intervals, converted to W m^{-2}, as for Caxiuaña, and the HOBO weather station recorded at two minute intervals.

At Tambopata, data analysis indicated a consistent difference in total radiation values between the HOBO weather station and the BF3 sunshine sensor (an average overall difference of 89 W m^{-2} but increasing to 120 W m^{-2} under clear sky conditions). This is probably due to degraded sensitivity in the HOBO weather station radiation sensor. In order to derive a radiation climatology from previously collected HOBO weather station data, commencing March 2005, it was therefore necessary to adjust them to the

Table 1
Radiation data site locations, recording devices and temporal range and resolution information.

Instrument	Site	Location	Radiation type	Temporal range	Temporal resolution (min)
BF3 sunshine sensor, Caxiuaña, Brazil	Tower top above canopy: 50 m	1.7378S, 51.4531W	Total and diffuse radiation	August 04–February 05	30
				March 05–April 06	2
HOBO weather station, Tambopata, Peru	Clearing with trees ~15% above horizon in all directions	12.783S, 69.283W	Total radiation	March 05–June 05	2
				September 05–June 06	
BF3 sunshine sensor, Tambopata, Peru	Clearing with trees ~15% above horizon in all directions	12.783S, 69.283W	Total and diffuse radiation	July 2006	1

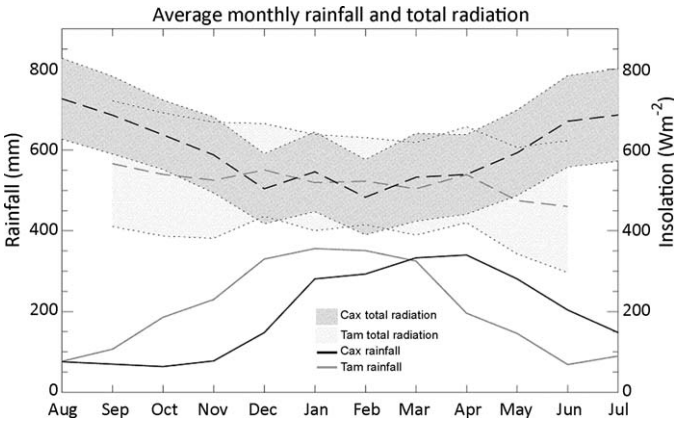

Fig. 2. Seasonal rainfall and total radiation patterns for Caxiuaña and Tambopata. The rainfall data are from the Climate Research Unit (CRU) representing mean 1961–1998 monthly precipitation (New et al., 1999). The radiation data are monthly daytime means from the HOBO weather station (Tambopata) and BF3 sensor (Caxiuaña). The variation in radiation is indicated by the shading, which represents one standard deviation of daily radiation above and below the mean.

sunshine sensor data using a simple calibration:

$$\mathrm{HOBO_{adj}} = \frac{\mathrm{HOBO_{or}} - 9.1}{0.84} \quad (1)$$

where $\mathrm{HOBO_{adj}}$ are the adjusted data and $\mathrm{HOBO_{or}}$ the original observed data. This formula was derived through regression of the HOBO against the BF3 data, using the period covered by both datasets.

3. Characterisation of solar radiation regimes at the study sites

The wet season in Caxiuaña is December–April and the dry season August–October; for Tambopata the wet season is November–April and the dry season June–August. Fig. 2 shows the seasonal rainfall and S_t patterns for the two sites. The S_t regimes for the two sites are similar in terms of magnitude but vary slightly at different times across the year.

Fig. 3 gives an overview of the average daily radiation regimes on a month-by-month basis at the two sites using all available data: August 2004 to April 2006 for Caxiuaña, Brazil (Fig. 3a), and March 2005 to July 2006 (excluding July and August 2005, where logger failure meant data were not recorded) for Tambopata, Peru (Fig. 3b). There is a clear annual cycle at Caxiuaña for S_t and diffuse radiation. S_t is highest and S_d lowest in the mid dry season (August), and S_d is highest and S_t lowest in the wet season (February). This is as expected given seasonal changes in cloud cover. As Tambopata is located further south from the Equator, there is less seasonal fluctuation in total radiation as during the dry season here the sun is overhead in the northern tropics and the resultant low sun angle effect offsets the effect of reduced cloud cover. Total annual incoming solar radiation is a little higher at Caxiuaña than Tambopata, mainly due to the higher dry-season sunshine at Caxiuaña.

A more detailed examination of the patterns and relationship between S_t and S_d used one-minute data across three weeks at the start of the dry season at the Peru site (Fig. 4). The mean S_t between 09:00 and 16:00 here is approximately 400 W m^2 and mean S_d is over 100 W m^2 for the same time interval. S_d increases in both absolute and relative terms on cloudy days, illustrating that S_d can vary significantly across a day and within a season.

We explored differences in the S_t and S_d regimes at different times of day through the seasonal cycle at both sites. At Tambopata, S_t was lowest in the mornings in June and highest in September. In the afternoon, a less clear, but different, seasonal

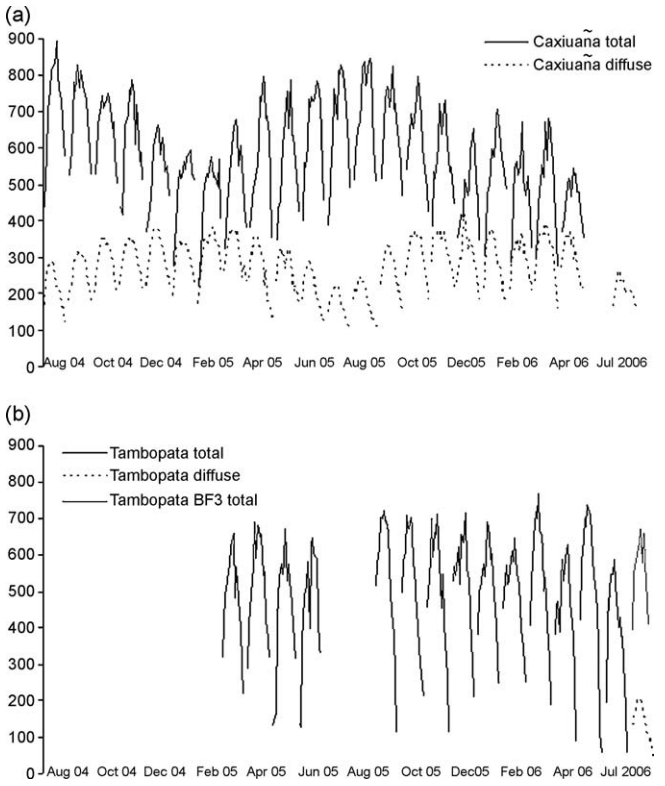

Fig. 3. Average daily cycle of total and diffuse radiation for each month at the two sites: (a) Caxiuaña and (b) Tambopata. Based on thirty minute interval (point, not average) data. The Tambopata total radiation data are from the corrected HOBO weather station apart from July 2006 which are from the BF3 sensor. Diffuse radiation data at Tambopata were only collected in July 2006.

cycle is apparent, with the lowest point in October/November and the highest in June. Similarly for Caxiuaña, the S_t in the mornings was lowest in May/June and peaked in August/September while the afternoon S_t was lowest from February to April and highest in July and August. S_d in Caxiuaña showed little difference between morning and afternoon with the lowest values in July/August and the highest in November and March/April.

The daily pattern of S_d/S_t for Tambopata is the opposite of that of Caxiuaña, perhaps due to the diurnal convection system across the Amazon basin (e.g., Machado et al., 2004) and the westward continental cloud movement during the day (Silv Dias et al., 2002). However, most places are cloudier in the afternoons and the unusual pattern at Caxiuaña may be because of its proximity to the generation point of Atlantic squall lines.

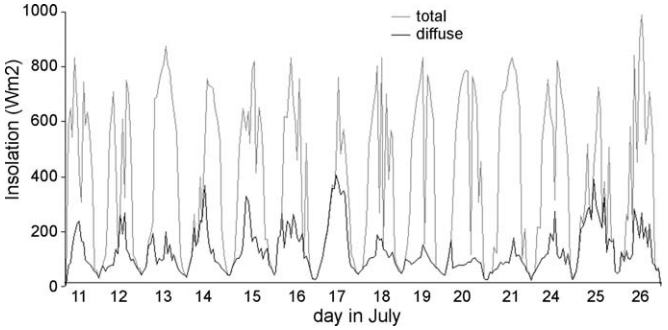

Fig. 4. Dry season total and diffuse radiation for Tambopata, Peru, thirty minute interval (point) data, 07:00–16:30, 11–26 July, 2006.

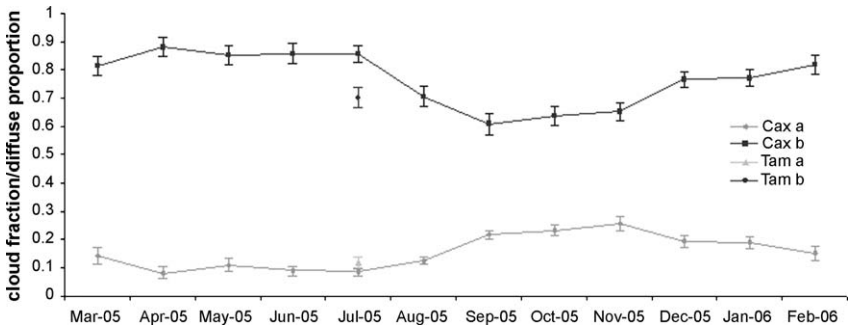

Fig. 5. Annual cycle of monthly regression parameters: a = constant (intercept) and b = cloud fraction coefficient (5th and 95th CI included). Tambopata July 2006 values included for comparison. These correspond with the Caxiuaña August values—the equivalent stage of the dry season.

4. Relationship between cloud fraction and diffuse radiation

4.1. Cloud fraction proxy and diffuse proportion ratios

As there are no cloud observations for our study sites, we develop a new cloud fraction proxy using high temporal resolution radiation data. We first estimate two minute S_t radiation values at both sites using Campbell and Norman's (1998) formulation:

$$S_t = [S_{po}\,\tau_m \cos\psi] + [0.3(1-\tau_m)S_{po}\cos\psi] \quad (2)$$

where S_{po} = extraterrestrial flux density ($\sim$1367 W m^{-2}), τ = atmospheric transmittance, ψ = zenith angle.

Cos ψ = sin Φ_L sin δ + cos Φ_L cos δ cos θ, where Φ_L = latitude, δ = solar declination angle = 23.4 cos(360(DOY + 10)/365), θ = hour angle of sun $\sim$ 15(12 − h); where h is local solar time in hours, = time + longitude/60, and m, air mass number, =1/cos ψ, DOY = - day of year. This formula is widely used as a standard calculation for the total of direct beam and diffuse radiation received at canopy level (e.g., Spitters et al., 1986; Campbell and Norman, 1998).

The ratio between calculated S_t and observed S_t is then used as a proxy for cloudiness: if observed/calculated $S_t < 0.8$ then the two minute interval is considered to be cloudy; if observed S_t/calculated $S_t > 0.8$ the interval is classed as cloud-free (see Fig. S1 in supplementary material for an example). The binary two minute data are then averaged to provide an hourly cloud fraction estimate. This approach differs from earlier work where the clearness index was used directly to predict diffuse proportion (e.g., Roderick, 1999; Erbs et al., 1982; Liu and Jordan, 1960).

Next, diffuse proportion (S_d/S_t) is calculated from the surface radiation measurements, and hourly percentages of the diffuse proportion are regressed against hourly cloud fraction. At both sites there is a very good linear relationship between our cloud fraction proxy and diffuse radiation proportion (R^2 of 0.92 and 0.94 for Caxiuaña and Tambopata, respectively), as the overall regression of diffuse proportion on cloud fraction for all months available shows (Fig. S2).

4.2. Seasonal variation in regression relationship between cloud fraction and diffuse proportion

We next investigate whether the relationship between cloud fraction and diffuse radiation varies with the seasonal cycle by repeating the regression on a month-by-month basis, for Caxiuaña (we only have partial dry season data for Tambopata). The regression intercept, which represents S_d/S_t under cloud-free conditions, shows a strong, statistically significant, seasonal cycle, with a maximum occurring during the dry season (Fig. 5). The Tambopata July 2006 values are included for comparison and match closely the Caxiuaña August/September values, an equivalent point in the seasonal cycle. The clear sky S_d/S_t is lowest in the late wet season/early dry season, and increases slowly from the end of the rainy season to a peak at the end of the dry season. The slopes of the monthly regressions follow a pattern that is the inverse of the intercept. This indicates that for a given cloud fraction, S_d/S_t is higher in the rainy season, most likely because higher values of cloud height and optical thickness increase scattering. However, in clear sky conditions, the dry season S_d/S_t is higher, most likely because of higher abundance of atmospheric aerosols.

5. Model for predicting diffuse radiation proportion

The good correlations between cloud fraction and diffuse proportion suggest that it should be possible to develop a predictive model.

We fit and evaluate three alternative model formulations for S_d/S_t.

$$\frac{S_d}{S_t} = a + b\,cl \quad \text{(Model 1)}$$

$$\frac{S_d}{S_t} = b\,cl + \frac{c}{\cos(\theta)} \quad \text{(Model 2)}$$

$$\frac{S_d}{S_t} = \frac{a + b\,cl}{\cos(\theta)} \quad \text{(Model 3)}$$

where a = constant (intercept), b = slope, cl = cloud fraction, c = coefficient and cos(θ) = cosine zenith angle. The model parameters have a physical interpretation: a represents the diffuse fraction under clear sky conditions, and is thus a function of humidity and aerosol content; b is the increase of diffuse radiation per unit increase in cloud amount and is this related to cloud opacity and cloud density, and; c is a coefficient of sensitivity to the zenith angle of the sun.

We attempt to account for the seasonal variation in diffuse radiation by including cosine zenith angle (θ) as an explanatory variable in Models 2 and 3. Zenith angle is the angle between the sun at any time and the zenith or overhead point, and thus varies with season and time of day. Its inclusion in the model represents an attempt to account for the changing probability, for any particular cloud fraction, of sunlight being scattered at different sun angles. Note that the regressions using zenith angle are hourly and based on day of year plus hour of day.

We test the models by using (randomly selected) two-thirds of the Caxiuaña data to fit each model, and validate it with the remaining third. Table 2 gives the model test results, which indicate that Models 1 and 2 are similarly robust: the R^2 values for application of the model to the data are expectedly high as this is an empirically fitted model. Also shown are the total mean square

Table 2
Model test results, parameter estimate values, MSE and systematic/unsystematic error comparisons. 'Calibration' refers to the two-thirds of the data (randomly selected) used to derive the model; 'validation' the remaining third, against which the derived model is tested, and 'full dataset' the results, including the systematic/unsystematic error analysis, for the model using all the data. The final parameters are very close to the calibration parameters and the systematic error is slightly higher in Models 2 and 3 than Model 1. Correlation and standard error values for the application of the models to the Tambopata data are included.

	Model 1	Model 2	Model 3
Calibration			
R^2	0.92	0.93	0.85
MSE	0.0042	0.0145	0.0537
Systematic MSE	0.0012	0.0143	0.0469
Unsystematic MSE	0.0031	0.0002	0.0069
Parameter estimates			
a	0.12	0.097	0.102
b	0.83	0.83	0.67
Validation			
R^2	0.92	0.93	0.84
MSE	0.0273	0.0464	0.0474
Systematic MSE	0.0262	0.0458	0.0474
Unsystematic MSE	0.0011	0.0006	0.0000
Full dataset			
R^2	0.92	0.93	0.84
MSE	0.0214	0.0208	0.0069
Systematic MSE	0.0106	0.0207	0.0066
Unsystematic MSE	0.0108	0.0001	0.0003
Parameter estimates			
a	0.12	0.099	0.105
b	0.83	0.83	0.66
Tambopata validation			
R^2	0.94	0.94	0.92
SE	0.072	0.071	0.096

error, and the systematic and unsystematic components of this error (after Wilmott, 1981); total error is relatively small. Residual plots (p–p plots) follow normal distribution, indicating a robust regression model. The parameter estimates change little between use of calibration, validation and full dataset. The inclusion of zenith angle does not significantly add predictive power and we select the simpler linear regression model, which also has a lower systematic than unsystematic error. When plotted against observed diffuse radiation this linear model gives a good overall prediction of S_d, with a small dry season over-prediction (Fig. 6a). The model predicts well where the S_d/S_t is high, but tends to over predict at times when the diffuse proportion is lower (dry season afternoons). The model also predicts well when applied to Tambopata (dry season) data (Fig. 6b), which increases confidence that the general annual model we formulate here is applicable across the wider Amazon region.

6. Satellite data cloud fraction and modelling

6.1. Satellite cloud data

In order to apply the model at the regional scale, to provide an Amazon-wide diffuse radiation climatology, satellite data could be used to provide cloud fraction proxy values. Long-term satellite-based cloud fraction data are available for the International Satellite Cloud Climatology Project (ISCPP; http://isccp.giss.nasa.gov/overview.html). These data offer the opportunity to estimate the spatial patterns of diffuse radiation over the wider Amazon using the relationship we have derived and tested at our field sites. The ISCCP DX product is based on data collected by polar and geostationary satellites, and is a cloud/cloud free value based on a cloud fraction algorithm, analysed per pixel, each pixel being

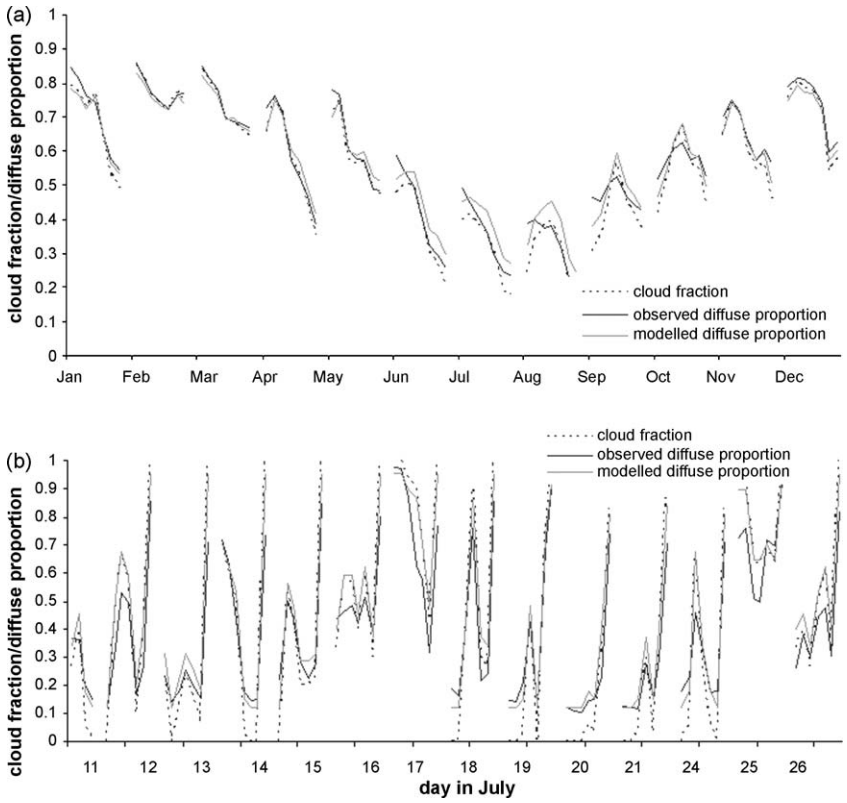

Fig. 6. (a) Comparison of modelled and observed diffuse radiation proportion for (monthly) average daily cycle at Caxiuaña, for one-hourly time step, 09:00–15:00. Cloud fraction is included for comparison. (b) Comparison of modelled and observed dry season diffuse radiation proportion at Tambopata, Peru, for one-hourly time step, 09:00–15:00, using model developed for Caxiuaña, Brazil data. Cloud fraction included for comparison.

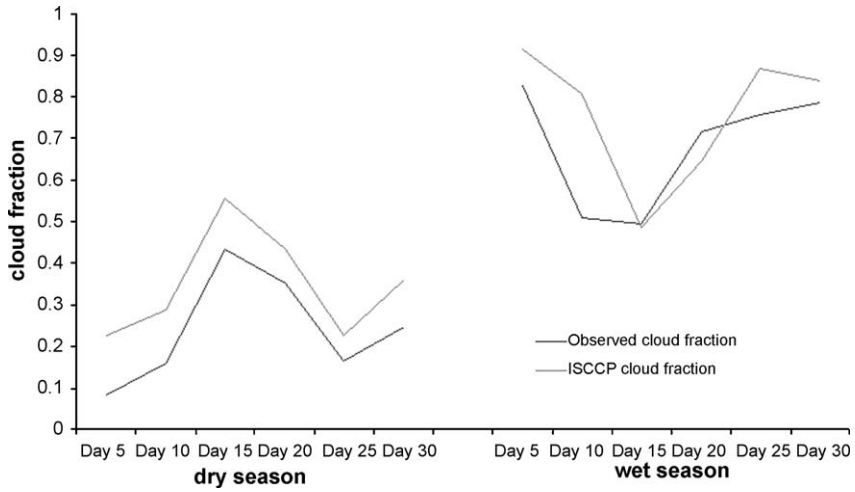

Fig. 7. ISCCP-derived and observed cloud fraction proxy for Caxiuaña. Shown here are the 5-day averages for daily values for a month in the dry season and a month in the wet season.

30 km × 30 km. These per-pixel values are then aggregated to cloud fraction estimates three times a day, during daylight hours: 09:00, 12:00 and 15:00 local (Caxiuaña) time. Because the satellite data are recorded on UTC/GMT time, we use the satellite data times equivalent to the local data times: 12:00, 15:00 and 18:00 UTC/GMT. For both the satellite-derived and our observed cloud fraction estimates, these data represent three-hourly means centred on (local times) 09:00, 12:00 and 15:00.

6.2. Comparison of satellite-derived and observed cloud fraction data

We first compare observed and satellite-derived cloud fraction, exploring different options here to establish the best way of using the satellite data. We assess the agreement (correlation) between satellite and observed data in three ways: (i) as nearest point, where the satellite data from the coordinates nearest the station were compared directly with the observed; (ii) using the average of the satellite data over a 0.5° pixel that contained the station, and; (iii) using an interpolation of all available satellite values within the same 0.5° pixel. For Caxiuaña (and also for Tambopata), the 0.5° area-averaged satellite data gave the best correlation with the observed data. We also experimented with correlating the satellite and observed data both for the three times separately and as daily averages. These were grouped and tested in four ways: using every day, 5-day means, 10-day means and monthly means. The correlations indicated that daily averages for 5-day means gave the best overall correlations with the observed data (all correlation results are presented in Table S1). The results from the various aggregations do not vary from each other greatly—but sample size differences mean that the 5-day data have six times more points than the monthly data. The correlation was also tested with the seasonal cycle removed, but this made no significant difference. Fig. 7 gives an example of these correlations, using the 5-day daily average, for a dry season and a wet season month.

The ISCCP cloud fraction midday values are systematically higher than our observed cloud fraction proxy values in the late wet and early dry season at Caxiuaña. These apparently systematic biases in the two datasets may be as a result of differences in the original data sources, namely ground radiation and satellite multi-sensor data. Another factor may be that the ISCCP data are a single binary value for the three-hour period whereas the observed cloud fraction proxy values are averaged from individual two-minute cloud fraction values.

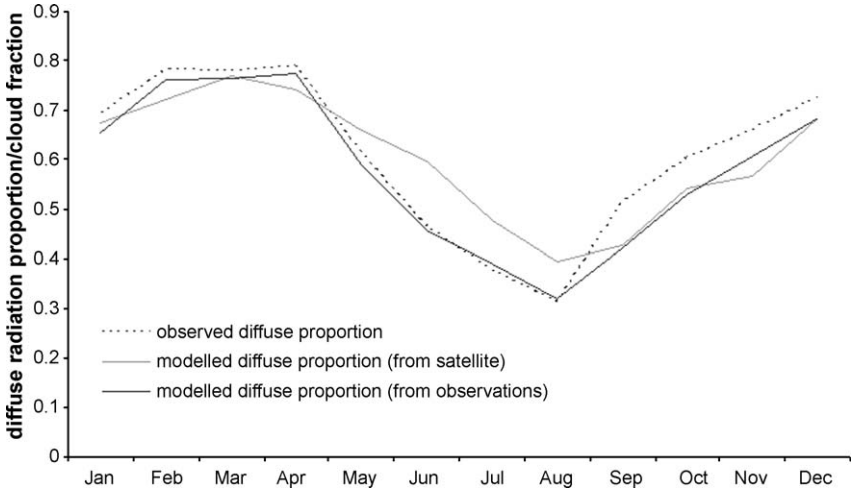

Fig. 8. Comparison of modelled diffuse proportion (using satellite derived cloud fraction); monthly means, and observed diffuse proportion for Caxiuaña (January–April 2006 data used). ISCCP-derived and observed cloud fraction included.

6.3. Development and application of satellite-derived cloud fraction model

Despite some systematic difference between satellite and ground cloud fraction data, their good correlation suggests that the satellite data are suitable for estimating diffuse proportion over the wider Amazon. As ISCCP data are available three times a day, we evaluate our model at this temporal resolution, by first establishing that S_d/S_t averages can be calculated from three equivalent time of day observed cloud fraction values. We aim to calculate the whole daily S_d/S_t using these three time points and assume, based on daily radiation curves, that 09:00 and 15:00 data represent 25%, and 12:00 data 50% of S_d/S_t. We test that monthly averages of 09:00, 12:00 and 15:00 data are sufficient to predict S_d/S_t, and compare our calculated values with the observed averages, both monthly and daily (Fig. S3); in both cases, three hourly data derived from instantaneous measurements are highly correlated with three hourly average data. The strength of this relationship does not appear to have a seasonal pattern; from May to August it remains fairly constant, while for the other months it fluctuates slightly. This result indicates that a model based on data from these three time slots should be appropriate for predicting daily average diffuse radiation proportion.

We then derive the model using satellite data using 5-day means of daily averages, which have the best correlation with ground measurements, as discussed in Section 6.2. The model follows the same formulation as before, but with coefficients that differ slightly: $a = 0.15$ (± 0.07), $b = 0.71$ (± 0.10). Application of the model gives a good representation of S_d/S_t—the seasonal trend is picked up well, with the wet to dry season transition showing the largest discrepancy between the observed and modelled S_d/S_t. The model over-estimates S_d/S_t in this period and slightly under-estimates or is very close to the observed S_d/S_t throughout the rest of the annual cycle (Fig. 8). The annual means are again very similar, (the satellite-derived modelled diffuse radiation values were about 1% higher on average across the year). Finally, we apply this model to the Tambopata data (Fig. S4). Although there are only several days available where both the observed S_d/S_t and satellite-derived cloud fraction are complete, the model gives a good approximation of S_d/S_t.

7. Discussion

The cloud fraction we derived from observed S_t/calculated S_t is a robust proxy that can be effectively used in our linear regression model to predict diffuse radiation. The model performed well on the whole, with a seasonal weakness that seems to be aligned with dry season anthropogenic activity (e.g., biomass burning); this is likely to due aerosols affecting diffuse proportion, but there are no data of sufficiently high spatial resolution to test the relationship at this stage. The increase in clear sky diffuse radiation in the dry season is likely to be caused by a build-up of atmospheric aerosols and dust, the former partially associated with biomass burning. Indeed, there are well documented spikes in the aerosol loading in South America during August and September (Holben et al., 2001). It follows that the wet season decrease in clear sky diffuse radiation is likely due to reduced atmospheric scattering as aerosol concentrations are lowered by rainfall washout. The diffuse radiation trend may also be a function of changing cirrus cloud conditions, though uncertainty surrounds the quantification of scattering here as cirrus clouds are not structurally uniform and are made up of ice crystals which vary in shape and size (Kinne, 2008).

In the Caxiuaña rainy season, when cloud fraction is high, diffuse radiation is higher (than during the dry season) due to increased cloud height and number and, therefore, increased scattering of radiation (see Section 4.2). In August, at the onset of the dry season, when cloud fraction is high (between 0.8 and 1), S_d/S_t is lowest, 0.70. S_d/S_t is highest in February at the start of the wet season, 0.92. Correlation between S_d/S_t and cloud fraction is therefore lowest at the onset of the dry season (hence the least accurate model prediction at that time). However, the inclusion of zenith angle does not capture optical thickness related to aerosols and clear sky particulates and therefore does not significantly add predictive power and the simpler linear regression model was most robust. This spatially variable nature of radiation seasonality is problematic to incorporate into a model that can be applied across a large region such as the Amazon basin, though the generalised model formulated here can predict S_d/S_t quite accurately in two separate locations and is therefore more widely applicable. The dry season in Tambopata starts one to two months earlier than the dry season in Caxiuaña, hence in Fig. 5 the values at dry season onset are almost identical for the two sites. The similarity in parameters once the shift in timing of the dry season is taken into account suggests that the parameters a and b may be of general utility, but this should be tested at further sites as new data emerge.

This work includes a new evaluation/validation of satellite-derived cloud fraction data. These data follow the annual trend of the observed data, and the annual means and totals are similar, as is then also the case for S_d/S_t modelled using both satellite cloud fraction inputs and observed cloud fraction data. Application of the model to (limited) data from another site indicates that it has great potential for the investigation of annual patterns in diffuse radiation across a larger area using satellite data inputs. The development of a model using satellite cloud fraction means that we can estimate S_d/S_t at different sites and for different time periods (e.g., annual cycles) using only satellite-derived cloud data. However, as it is beyond the scope of this study to include aerosol-related trends or variations in diffuse radiation, it is only cloud-related differences that can be assessed in this way. The new sensitivities in critical parameters we have shown could be evaluated in future with a more sophisticated model that incorporates aerosol (ground observed and satellite-derived) and cloud height.

In areas where there is no on-the-ground observation/recording, or historical records, of diffuse radiation, such as large tracts of tropical South America, this could be a useful method of providing diffuse radiation information that can then be used at an ecosystem level for investigating ecophysiological issues related to solar radiation regimes. In future work we intend to test for a relationship between changes in forest productivity and changes in diffuse radiation over time, using historical satellite cloud data and the model developed in this paper.

Acknowledgements

This work is part of a Brazil-led LBA (Large Scale Atmosphere-Biosphere) Programme. N. Butt's PhD studentship is funded though a NERC project (NE/B503384/1) and a Leverhulme Research Fellowship to O. Phillips. Y. Malhi is supported by the Jackson Foundation. Thanks to Paul Carter at NASA Langley Research Centre, and Gil Lizcano and Toby Marthews at Oxford University for their help with the acquisition and manipulation of the satellite data, and advice on radiation modelling formulae. We are grateful for the helpful comments from three anonymous reviewers.

Appendix A. Supplementary data

Supplementary data associated with this article can be found, in the online version, at doi:10.1016/j.agrformet.2009.12.004.

References

Ackerley, D.D., Bazzaz, F.A., 1995. Seedling crown orientation and interception of diffuse radiation on tropical forest gaps. Ecology 76 (4), 1134–1146.

Campbell, G.S., Norman, J.M., 1998. An Introduction to Environmental Biophysics. Springer, New York.

Collares-Pereira, M., Rabl, A., 1979. The average distribution of solar radiation—correlations between diffuse and hemispherical and between daily and hourly insolation values. Solar Energy 22, 155–164.

Erbs, D.G., Klein, S.A., Duffie, J.A., 1982. Estimation of the diffuse radiation fraction for hourly, daily and monthly-average global radiation. Solar Energy 28 (4), 293–302.

Gopinathan, K.K., Soler, A., 1995. Diffuse radiation models and a monthly-average, daily, diffuse data for a wide latitude range. Energy 20 (7), 657–667.

Holben, B.N., Tanré, D., Smirnov, A., Eck, T.F., Slutsker, I., Abuhassan, N., Newcomb, W.W., Schafer, J., Chatenet, B., Lavenu, F., Kaufman, Y.J., Vande Castle, J., Setzer, A., Markham, B., Clark, D., Frouin, R., Halthore, R., Karnieli, A., O'Neill, N.T., Pietras, C., Pinker, R.T., Voss, K., Zibordi, G., 2001. An emerging ground-based aerosol climatology: aerosol optical depth from AERONET. J. Geophys. Res. 106 (D11), 12067–12097.

Kinne, S., accessed 2008. geo.arc.nasa.gov/sge/jskiles/fliers/all_flier_prose/cirrusclimate_kinne/cirrusclimate_kinne.html.

Lewis, S.L., Phillips, O.L., Baker, T.R., Lloyd, J., Malhi, Y.M., Almeida, S., Higuchi, N., Laurance, W.F., Neill, D.A., Silva, J.N.M., Terborgh, J., Lezama, A.T., Vasquez, R.M., Brown, S., Chave, J., Kuebler, C., Nunez, P.V., Vinceti, B., 2004. Concerted changes in tropical forest structure and dynamics: evidence from 50 South American long-term plots. Philos. Trans. R. Soc., Ser. B. 359, 421–436.

Liu, Y.H., Jordan, R.C., 1960. The interrelationship and characteristic distribution of direct, diffuse and total solar radiation. Solar Energy 4 (3), 1–19.

Machado, L.A.T., Laurent, H., Dessay, N., Miranda, I., 2004. Seasonal and diurnal variability of convection over the Amazon: a comparison of different vegetation types and large scale forcing. Theor. Appl. Climatol. 78, 61–77.

Muneer, T., Munawwar, S., 2006. Potential for improvement in estimation of solar diffuse radiation. Energy Convers. Manage. 47, 68–86.

Nemani, Ramakrishna R., Keeling, Charles D., Hashimoto, Hirofumi, Jolly, William M., Piper, Stephen C., Tucker, Compton J., Myneni, Ranga B., Running, Steven W., 2003. Climate-driven increase in global terrestrial net primary production from 1982 to 1999. Science 300, 1560–1563.

New, M., Hulme, M., Jones, P., 1999. Representing twentieth century space-time climate variability. I. Development of a 196190 mean monthly terrestrial climatology. Journal of Climate 12, 829–856.

Oliveira, P.H.F., Artaxo, P., Pires, C., de Lucca, S., Procópio, A., Holben, B., Schafer, J., Cardoso, L.F., Wofsy, S.C., Rocha, H.R., 2007. The effects of biomass burning aerosols and clouds on the CO_2 flux in Amazonia. Tellus 59B, 338–349.

Onset Corporation, accessed 2007. www.onsetcomp.com.

Orgill, J.F., Hollands, K.G.T., 1977. Correlation equation for hourly diffuse radiation on a horizontal surface. Solar Energy 19, 357–359.

Phillips, O.L., Vasquez, R.M., Arroyo, L., Baker, T.R., Killeen, T., Lewis, S.L., Malhi, Y., Monteagudo, A.L., Neill, D., Nunez, P.V., Alexiades, M., Ceŕon, C., Di Fiore, A., Erwin, T., Jardim, A., Palacios, W., Saldias, M., Vincenti, B., 2002. Increasing dominance of large lianas in Amazonian forests. Nature 418, 770–774.

Phillips, O.L., Baker, T.R., Arroyo, L., Higuchi, N., Killeen, T.J., Laurance, W.F., Lewis, S.L., Lloyd, J., Malhi, Y.M., Monteagudo, A., Neill, D.A., Nunez, P.V., Silva, J.N.M., Terborgh, J., Vasquez, R.M., Alexiades, M., Almeida, S., Brown, S., Chave, J., Comiskey, J.A., Czimczik, C.I., Di Fiore, A., Erwin, T., Kuebler, C., Laurance, S.G., Nascimiento, H.E.M., Olivier, J., Palacios, W., Patiño, S., Pitman, N.C.A., Quesada, C.A., Saldias, M., Lezama, A.T., Vinceti, B., 2004. Pattern and process in Amazon tree turnover, 1976–2001. Philos. Trans. R. Soc., Ser. B. 359, 381–407.

Roderick, M.L., Farquhar, G.D., Berry, S.L., Noble, I.R., 2001. On the direct effect of clouds and atmospheric particles on the productivity and structure of vegetation. Oecologia 129, 21–30.

Roderick, M.L., 1999. Estimating the diffuse component from daily and monthly measures of global radiation. Agric. Forest Meteorol. 95, 169–185.

Silv Dias, M.A.F., Rutledge, S., Kabat, P., Silva Dias, P.L., Nobre, C., Fisch, G., Dolman, A.J., Zipser, E., Garstang, M., Manzi, A.O., Fuentes, J.D., Rocha, H.R., Marengo, J., Plana Fattorie, A., Sá, L.D.A., Alvalá, R.C.S., Andraea, M.O., Artaxo, P., Gielow, R., Gatti, L., 2002. Cloud and rain processes in a biosphere-atmosphere interaction context in the Amazon region. J. Geophys. Res. 107 , doi:10.1029/2001JD000335.

Spitters, C.J.T., Toussaint, H.A.J.M., Goudriaan, J., 1986. Separating the diffuse and direct component of global radiation and its implications for modelling canopy photosynthesis. Part I: Components of incoming radiation. Agric. Forest Meteorol. 38, 217–229.

Wilmott, C., 1981. On the validation of models. Phys. Geogr. 2, 184–194.

Weiss, A., Norman, J.M., 1985. Partitioning solar radiation into direct and diffuse, visible and near-infrared components. Agric. Forest Meteorol. 34, 205–213.

Wood, J., Muneer, Tariq, Kubie, J., 2003. Evaluation of a new photodiode sensor for measuring global and diffuse irradiance, and sunshine duration. J. Solar Eng. 125 (1), 43–48.